

# Study of Effect of Gas Tungsten Pulse Arcing on Surface Modification of Martensitic Stainless Steel

Somnath Basu<sup>1</sup>, P. K. Ghosh<sup>2</sup>, J. S. Saini<sup>3</sup>

<sup>1</sup> Research Scholar at Uttarakhand Technical University, Dehradun, /Faculty, DITU, Dehradun, email: [basusom@gmail.com](mailto:basusom@gmail.com)

<sup>2</sup> Senior Professor, Department of Metallurgical and Materials Engineering, IIT Roorkee, email: [pragfmt@gmail.com](mailto:pragfmt@gmail.com)

<sup>3</sup> Professor, DIT University, Dehradun, , e-mail: [sainifme@gmail.com](mailto:sainifme@gmail.com)



DOI : <http://doi.org/10.22486/iwj/2017/v50/i2/146561>

## ABSTRACT

Heat energy generated from Gas Tungsten Pulse Arcing process has been used for surface modification of martensitic stainless steel. Arcing was carried out with varied pulse parameters with heat input maintained constant. Variations were observed in heating and cooling patterns of the fused zone. Their effects on fusion, solidification and consequent influence on microstructure of the fused material have been studied. The Temperature Vs. Time curve and isotherm of the fused zone have been analytically drawn. They are used to predict microstructural changes in the fused and adjacent heat affected zone of modified surface. The theoretical predictions are verified by the relevant observations on the modified surfaces. Improvement in hardness of fused zone compared to base material has been studied in conformity with the microstructural changes of the modified matrix.

**Keywords:** stainless steel, thermal analysis, fusion geometry, microstructure, hardness.

## 1.0 INTRODUCTION

Modification of surface properties of material is a common practice in various engineering applications requiring specific surface characteristics of any component over that of its core material to suit various service conditions. This can be achieved by modification of physical, chemical, mechanical and metallurgical characteristics of the surface of a metal. Apart from many sophisticated treatment like sputtering and treating by plasma, laser, ion and electron beam [1-6], the surface modification is commonly carried out by mechanical treatment, heat treatment, and fusion of the substrate as well as extra deposition on it [7-8]. It is also reported that surface fusion by gas tungsten arcing (GTA) can be precisely applied for appreciable surface modification up to significant depth of a metal substrate [9]. Gas Tungsten Pulse Arcing (GTPA) has been found as an effective method to achieve desired micro structural transformation. Suitability of GTPA is due to its

precisely controlled thermal distribution in the arcing system [10]. This has already been justified in the observation [11] of pulse gas metal arc welding (GMAW) which amply justifies the interruption in base metal fusion and its solidification influencing its microstructure under pulse current arcing.

GTPA can be operated at higher energy input due to its high peak current compared to GTA. But, due to lower mean current, net heating of the base material remains lower. Thus better heat control along with wider fusion zone and larger depth of penetration is achieved by use of GTPA [10]. The GTPA has the ability to control energy input as well as its distribution in the entire process of surface modification of the substrate by fusion [10]. It is primarily achieved by manipulation of the solidification behavior and nature of phase transformation in the matrix through a control over the depth of fusion.

In this work, GTPA process has been used for surface

modification of stainless steel which has relatively complex behavior of phase transformation that requires minute control of isotherms and thermal cycles of fusion and heat affected zone (HAZ). However, GTPA control is difficult due to presence of various simultaneously acting parameters like peak ( $I_p$ ) and base ( $I_b$ ) currents, duration of peak ( $t_p$ ) and base ( $t_b$ ) currents and pulse frequency ( $f$ ). This problem has been resolved by control of pulsed current process through a hypothetically derived dimensionless factor ' $\phi$ '. Ability of ' $\phi$ ' in controlling the pulsed current arcing process has already been justified in case of pulse GMAW and GTPA processes [11, 12]. Relation between ' $\phi$ ' and pulse parameters is expressed as follows:

$$\phi = [(I_b/I_p) f t_b] \dots\dots (1)$$

Isothermal curves and thermal cycles (time-temp curves) for arcing parameters have been analytically drawn with model proposed in earlier work [14] and used for prediction of microstructures. Micro structural analysis and corresponding changes in hardness of modified samples have been studied in order to optimize the pulse parameters of the GTPA process to get improved hardness of the modified surface.

**2.0 EXPERIMENTAL WORK**

Experiments were conducted on commercially available annealed 5 mm thick SS-410 (UNS NO S41000) stainless steel plate. The material was selected due to its relatively low hardness amongst the group of steels in ASTM 400 series and its air hardenable property. The physical properties and chemical composition of SS-410 are shown in **Table – I** and **Table – II** respectively.

Surface modification of the base material was carried out using GTPA carried out with the help of a 'Fronius' Magic wave 1700 pulsed TIG welding machine. A thoriated tungsten non

consumable 3.2 mm diameter electrode was used to generate the arc in direct current straight polarity (DCSP) mode. Shielding of the arcing process was done with Commercial argon. The gas flow rate was maintained at 18 L/min. The surface modification of work piece by controlled fusion was done by GTPA process without use of filler material on a coupon size of 150x75x5 mm. Before subjected to arcing the surface of the work piece was mechanically cleaned by rubbing with emery paper followed by wiping with acetone in order to further clean it from dust, grease, etc.

Pulse frequencies ( $f$ ) at 2, 4 and 6 Hz were used during GTPA. The pulse frequencies were selected based on an earlier work [11] demonstrating effectiveness of arcing with respect to surface modification of steel. Different peak and base currents with constant mean current ( $I_m$ ) of  $132 \pm 4$  A (**Table-III**) were used for GTPA. The arc voltage ( $V$ ), electrode travel speed ( $S$ ) and duty cycle were kept practically constant as 11 V, 1.5mm/s and 50% respectively. Input arc heat of  $7.28 \pm 0.24$  kJ/cm was calculated using the following formula:

$$\text{Arc heat input} = [(\eta \times A \times V) / S] \dots\dots(2)$$

where, the system efficiency  $\eta$  was considered as 0.75 [13]. During experiment the voltage ( $V$ ) fluctuation was observed as less than  $\pm 10\%$  and the current ( $A$ ) fluctuation was less than  $\pm 0.25\%$  as indicated at machine output display terminal. The surface modification by controlled fusion was done by single pass arcing at different parameters. Typical modified surface showing different zones are shown in **Fig.1 (a)** and **(b)**.

**Table-I : Physical properties of the base material**

Work Material	Density (kg/m <sup>3</sup> )	Melting Point (°C)	Thermal (W/m °C)	Sp. Heat (J/kg. °C)	Hardness (HV)
SS-410	7700	1530	28.7	460	160

**Table-II : Chemical composition of base material**

Work Material	Composition (in wt. %)						
	C	Mn	Cr	Si	S	P	Fe
SS-410	0.14	1.06	13.75	0.38	0.019	0.022	Remainder

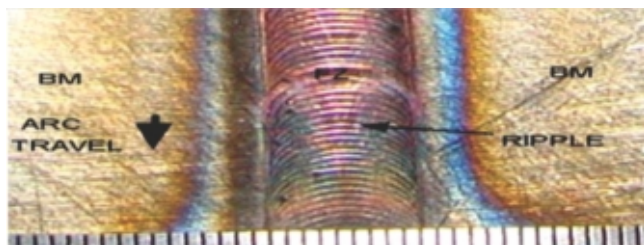


**Fig. 1(a) : Typical modified surface indicating different zones along arc travel line**

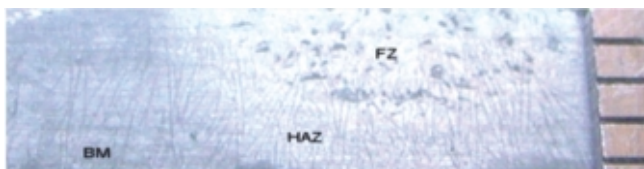


**Fig. 1(b) : Typical modified surface indicating fusion and HAZs across arc travel line**

**Table - III : Gas Tungsten Pulse Arcing parameters**

Sl. No.	Pulse arcing parameters					
	$I_p$ (A)	$I_b$ (A)	$I_m$ (A)	f (Hz)	$t_p = t_b$ (s)	$\phi$
1	170	86	128	2	0.250	0.25
				4	0.125	
				6	0.83	
2	164	98	131	2	0.250	0.30
				4	0.125	
				6	0.83	
3	158	110	134	2	0.250	0.35
				4	0.125	
				6	0.83	
4	152	122	137	2	0.250	0.40
				4	0.125	
				6	0.83	

The characteristics of the modified surfaces were studied on the samples machined out from a distance more than 15 mm from the arc initiation point along the arc travel line in order to ensure the stable temperature zone of fusion. Metallographic studies of the samples were carried out on its transverse surface to the arc travel line revealing penetration of the fusion zone and HAZ of the work piece as shown in **Fig.1 (b)**. The specimens were prepared by standard metallographic procedure of polishing with emery papers of different grit sizes followed by final polishing with diamond paste. Optical microscopic studies were carried out after electrolytic etching of the specimens in aqueous solution of 10 % oxalic acid. Vickers pyramid hardness (HV) was randomly measured by indentation at 10 kgf force with 15 s dwell time applied on the surface transverse to the arc travel line of each sample.

**3.0 THERMAL ANALYSIS OF FUSION**

The expression for estimation of increase in temperature ( $T-T_0$ ) in a plate having semi-infinite dimension due to a heat source having double ellipsoidal shape and moving at a velocity  $v$  is stated as [14]:

$$T-T_0 = \left[ \frac{3\sqrt{3}Q}{2\rho c\pi\sqrt{\pi}} \int_0^t \frac{dt'}{\sqrt{\{12a(t-t')+a_h^2\}\{12a(t-t')b_h^2\}}} \times \left[ \frac{A'}{\sqrt{12a(t-t')+c_{hf}^2}} + \frac{B'}{\sqrt{12a(t-t')+c_{hb}^2}} \right] \right] \dots (3)$$

where,  $T_0$  is initial temperature at  $t' = 0$  and final temperature  $T$  after  $t' = t$ .

$$A' = r_f \exp \left\{ \frac{3(x-vt)^2}{12a(t-t)+c_{hf}^2} - \frac{3y^2}{12a(t-t)+a_h^2} - \frac{3z^2}{12a(t-t)+b_h^2} \right\} \dots (4)$$

$$B' = r_b \exp \left\{ \frac{3(x-vt)^2}{12a(t-t)+c_{hb}^2} - \frac{3y^2}{12a(t-t)+a_h^2} - \frac{3z^2}{12a(t-t)+b_h^2} \right\} \dots (5)$$

Front and back proportion coefficients are

$$r_f = \frac{2c_{hf}}{c_{hf} + c_{hb}} \dots (6)$$

$$\text{and } r_b = \frac{2c_{hb}}{c_{hf} + c_{hb}} \dots (7)$$

The  $Q$  is arc heat transfer rate to the fused pool and  $\rho$ ,  $c$  and  $a$  are density, specific heat capacity and thermal diffusivity of work piece.  $a_h$ ,  $b_h$ ,  $c_{hf}$  and  $c_{hb}$  are the dimensions of double ellipsoid heat source for a location having at least 5% power density compared to that at the ellipsoid center (**Fig. 2**) [14]. As suggested in earlier work[14],  $c_{hf} = a_h$  and  $c_{hb} = 2c_{hf}$  were considered in this work. The parameters  $a_h$  and  $b_h$  have been selected based on the welding conditions and by comparing the best fit value of the width and depth of fusion zone respectively with their values calculated with assumed values of  $a_h$  and  $b_h$ .

Based on the Eqn. (3) - (7), a mathematical model was formulated to estimate temperature at a given point at different times with heat input of 7.28 kJ/cm. Accordingly the thermal cycle of fusion zone and HAZ adjacent to fusion line and isothermal curves around the arc extended up to HAZ in base material were estimated using the required data given in **Table -I** and **III** and drawn as shown in **Fig. 3** and **4** respectively.

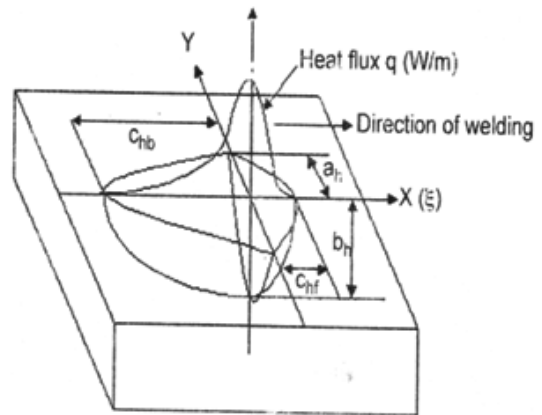


**Fig. 2 : Schematic diagram of double ellipsoidal heat source**

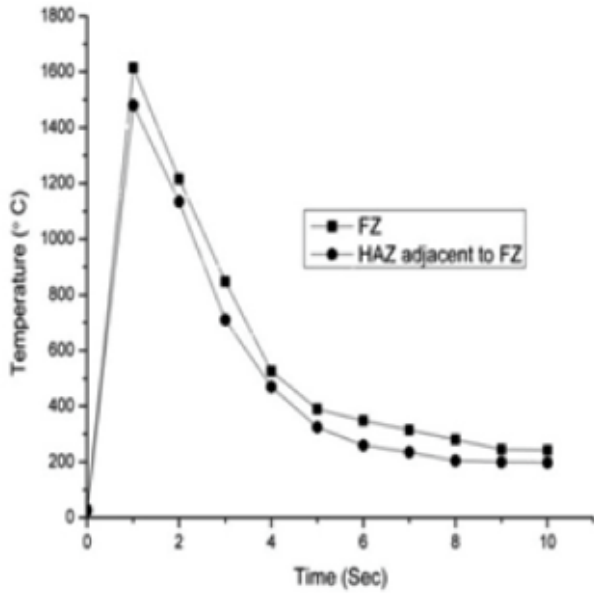


Fig. 3 : Thermal cycle of fusion zone and HAZ at heat input of 7.28 kJ/cm

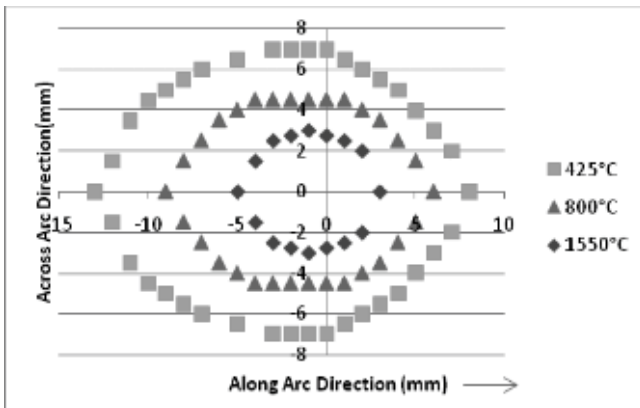


Fig. 4 : Isothermal curves of martensitic stainless steel surface at heat input 7.28 kJ/cm

#### 4.0 RESULTS AND DISCUSSIONS

##### 4.1 Appearance of fused surface :

The characteristics of ripple formation in fusion zone were examined for different 'f' and 'φ' values. Typical photographs of the ripples are shown in **Fig. 5**. The number, shape and width of the ripples indicate the changes in solidification pattern of fusion zone. The numbers of ripples per unit length indicate the solidification pattern of the fused surface. At a given 'f' of 2, 4 and 6 Hz the effect of 'φ' on nos. of ripples per unit length of fusion zone are shown in **Fig. 6**. It can be seen from **Fig. 6** that more numbers of ripples are formed per unit length with the increase of either 'f' or 'φ'. This has resulted in relatively finer surface ripples at higher 'f' and 'φ'.

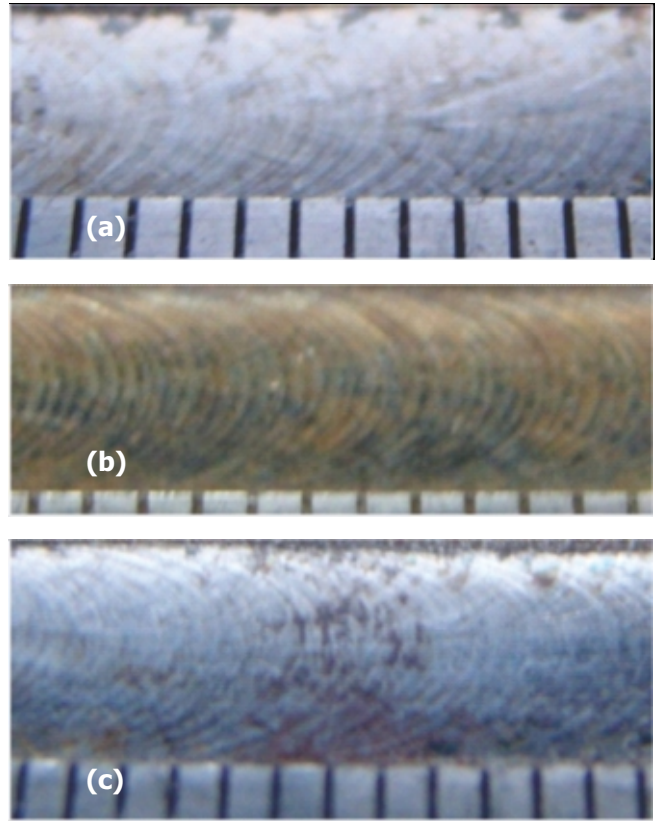


Fig. 5 : Typical characteristics of ripples on the fused surface of SS-410 at (a) 2 Hz, φ = 0.4 (b) 4 Hz, φ = 0.4 (c) 6 Hz, φ = 0.25 and heat input of 7.28 kJ/cm. Scale: in mm.

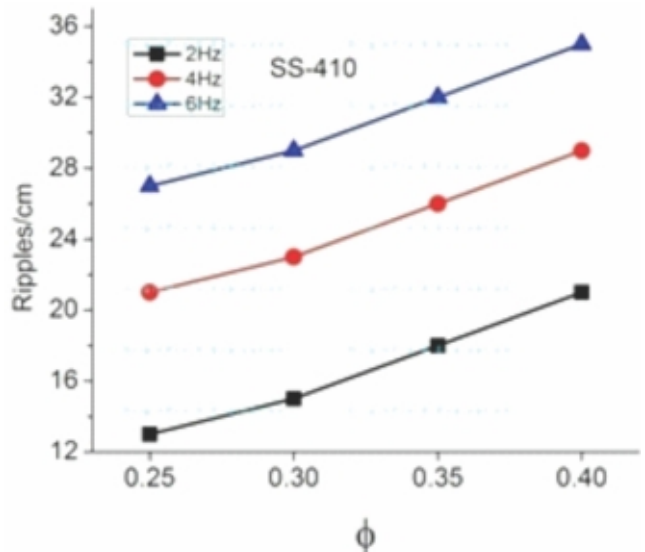
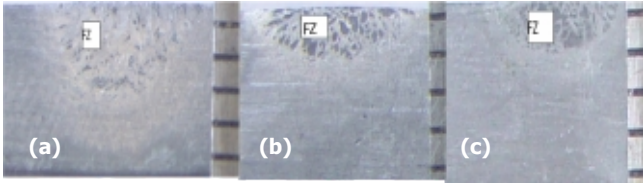


Fig. 6 : Effect of pulse frequency and φ on ripple concentration per unit length of fused surface of SS-410 at a given heat input 7.28 kJ/cm.

The change in depth of penetration at different pulse parameters is typically shown in **Fig. 7**. From **Figs. 7 (a)** and **(b)**, it appears that at a given 'f' penetration of fusion zone increases with lowering of 'φ'. Again it is evident from **Figs. 7 (b)** and **(c)** that at a given 'φ' penetration increases with lowering of pulse frequency.



**Fig. 7 : Typical surface appearance of zones across the arc travel line at different parameters (a) 2 Hz, φ = 0.3 (b) 2 Hz, φ = 0.4 and (c) 6 Hz, φ = 0.4; Scale: in mm.**

**4.2 Fusion zone solidification pattern**

The cooling rate and solidification behavior of fusion zone have been analyzed by studying the characteristics of ripple formation on the fused surface following the procedure as reported earlier [10].

The geometric approach of the analysis of ripple characteristics has been schematically shown in **Fig. 8**.

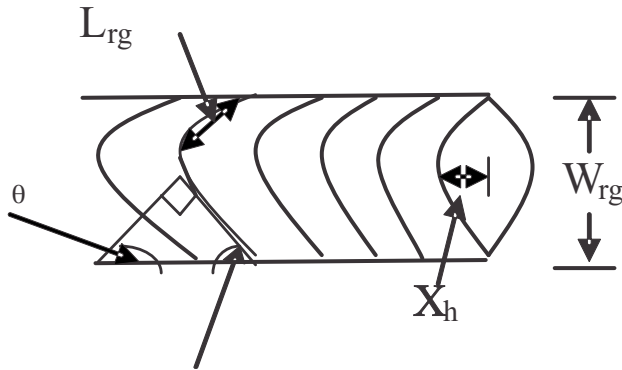


**Fig. 8 : Schematic diagram of different features of ripples on fused surface.**

The analytical expressions used for cooling rate estimation and the resulting characteristic features of solidification of the fusion zone, primarily with respect to the growth rate of primary solid, are stated below in Eqn. (8)-(12).

Ripple lag ratio ( $R_{rg}$ ) =  $L_{rg} / W_{rg}$  ... (8)

Growth Rate ( $R_c$ ) =  $S \cos Y$  ... (9)

Temperature gradient for solidification ( $G$ ) =  $T_m / X_{hw}$  ... (10)

Cooling Rate ( $C_r$ ) =  $GR_c$  ... (11)

and  $\phi = \tan^{-1} (W_{rg} / 2 L_{rg})$  .... (12)

where,  $L_{rg}$  is ripple lag length,  $W_{rg}$  is molten pool width,  $T_m$  is base material melting temperature and  $X_{hw}$  is distance from heat source to rear of the weld pool. All quantitative measurements on the fused surfaces were done with Adobe Photoshop 7 applied on fusion zone photos. The effect of 'φ' on fusion zone cooling rate by changing 'f' is shown in **Fig. 9**. Similarly the effect of 'φ' on primary solid growth rate in the fusion zone by changing 'f' is shown in **Fig. 10**. It has been observed that there is significant increase in cooling rate as well as primary solid growth rate for both cases (a) increasing 'φ' and maintaining 'f' constant and (b) increasing 'f' and maintaining 'φ' constant.

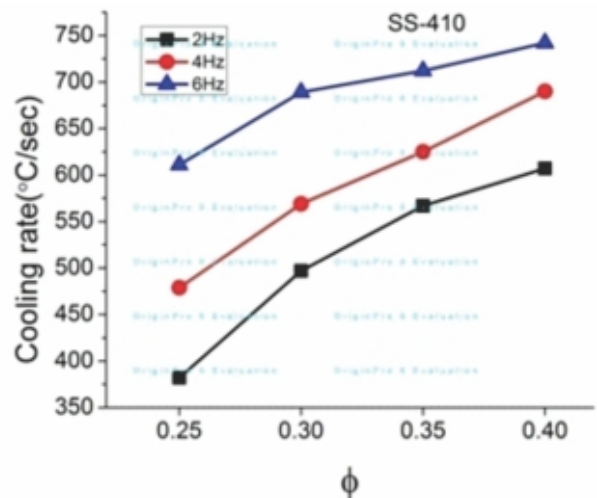


**Fig. 9 : Effect of φ on cooling rate estimated from appearance of ripples on fused surface during arcing at different pulse frequencies at a given heat input 7.28 kJ/cm.**

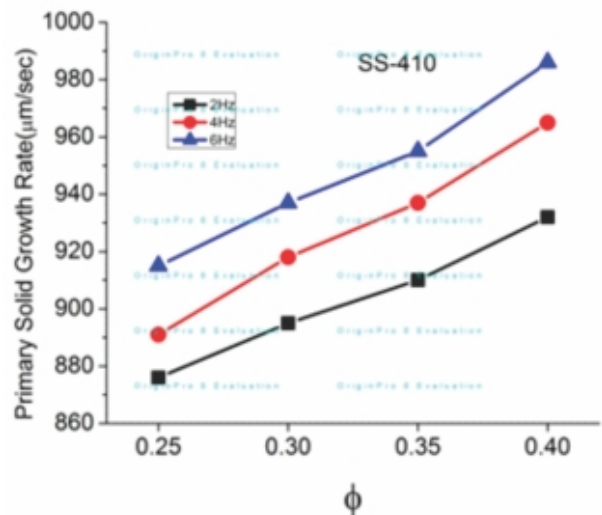


**Fig. 10 : Effect of φ on primary solid growth rate estimated from appearance of ripples on fused surface during arcing at different pulse frequencies at a given heat input 7.28 kJ/cm.**

The relatively low cooling rate at lower 'f' may be attributed to availability of comparatively larger time for heat dissipation in between pulsed arcing at low frequency. It reduced the temperature gradient of fusion zone to its relatively large area of hot surrounding heat sink. The predomination of the ability of heat extraction from the fusion zone based on thermal gradient between the location of arcing and its surroundings gradually became more active at higher frequency of arcing. This may have primarily happened due to availability of relatively less time for heat dissipation in between successive pulses creating a relatively shorter hot surrounding and a closer active heat sink. At a particular 'f', cooling rate increase with increase of ' $\phi$ ' may have attributed to less heat buildup in fused pool [10] that kept the surrounding heat sink more active. The earlier work [12] has explained that the primary reason for change in heat buildup as a function of ' $\phi$ ' is interruption in deposition of fused metal in Pulsed GMAW. In the same line of understanding of the effect of interruption in arcing, the solidification behavior of melt in GTPA process may be understood from its thermal balance. The heat buildup in the fusion zone varied with ' $\phi$ ' due to change in pattern of interruption of arcing influencing the repetitive process of fusion, partial solidification of melt and fractional remelting of primary solids. At low 'f' (2Hz), the rate of cooling rate increase with the increase of ' $\phi$ ' was more compared to that of higher 'f' values of 4 and 6 Hz as shown in **Fig.9**. The cooling rate at 2Hz varied from 382 °C/s at  $\phi=0.25$  to 605 °C/s at  $\phi=0.4$ , whereas the corresponding values at 6 Hz are 611 °C/s and 740 °C/s respectively. Such variation can be understood by considering the competitive aspect of heat buildup as a function of ' $\phi$ ' and available scope of heat dissipation at low 'f'. The increase of primary solid growth rate as a function of ' $\phi$ ' and 'f' (**Fig. 10**) appeared to be in agreement to the pattern of cooling rate. More cooling rate and primary solid growth rate promoted formation of comparatively finer matrix morphology in the fusion zone.

#### 4.3 Geometry of modified zone

Effect of ' $\phi$ ' on width of the fusion zone and depth of penetration (fusion) observed with heat input of 7.28 kJ/cm and with pulse frequency of 2, 4 and 6 Hz are shown in **Figs. 11 (a)** and **(b)** respectively.

It appears from **Fig 11 (a)** that if ' $\phi$ ' is increased with 'f' kept unchanged and 'f' is increased with ' $\phi$ ' kept unchanged there is appreciable reduction in the width of the fusion zone though

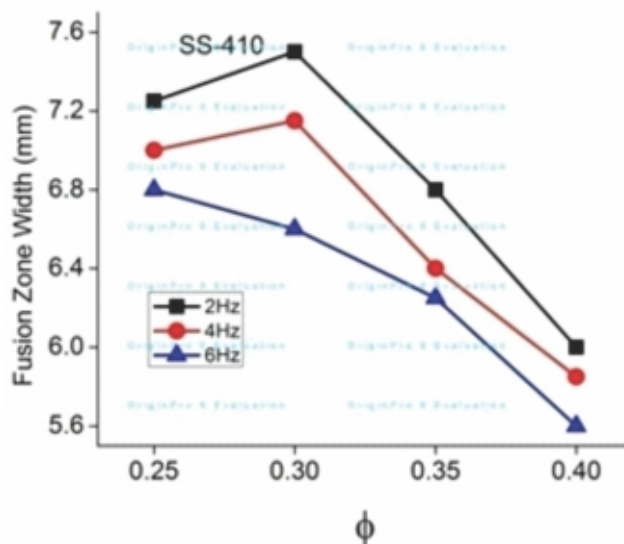


**Fig. 11(a)**

heat input is kept practically constant. This is happened to be in agreement with an earlier work [10] which also indicates the lowering of heat buildup in fusion zone with the increase of ' $\phi$ ' and 'f'. According to the theoretical estimation, the width of fusion zone at the given heat input of 7.28 kJ/cm has been found as 6 mm, whereas the measured values were between 5.6 to 7.5 mm as a function of ' $\phi$ ' and 'f'. The minimum fusion zone width was 5.6 mm at  $f=6$  Hz and  $\phi = 0.4$  while its maximum value was 7.5 mm at  $f=2$  Hz and  $\phi = 0.3$ . At heat input of 7.28 kJ/cm the effect of ' $\phi$ ' on fusion zone depth observed during the pulsed arcing at 2, 4 and 6 Hz is shown in **Fig.11 (b)**. The highest depth of 2.1 mm was found at  $f=2$  Hz and  $\phi = 0.25$  while the lowest value of 1.75 mm was found at  $f=6$  Hz and  $\phi = 0.4$ . Thus, at a given heat input, both width and depth of fusion of fusion zone can be changed by varying pulse parameters of GTPA. This affects the solidification behavior of fusion zone and consequently its microstructure. Change in solidification behavior is also evident from nos. and shapes of ripples formed on solidified fused surface already discussed at section 4.1. A relative lowering of fusion zone width with decrease of ' $\phi$ ' from 0.3 to 0.25 may have happened due to some predominant compromising effect of ' $\phi$ ' in reduction of heat buildup in fusion over the effect of 'f' on enhancement of the same up to certain extent.

#### 4.4 Microstructural evaluation

Typical microstructure of the base material has been shown in

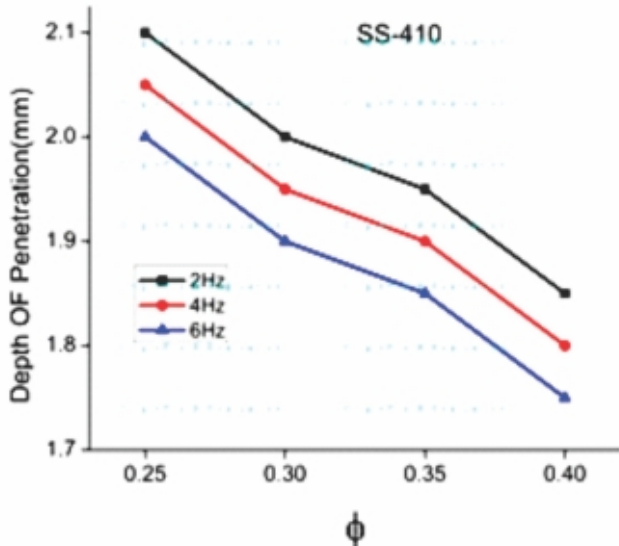


Fig. 11 (b)

Fig.11 : Effect of  $\phi$  on the measured (a) width (b) depth of penetration in SS-410 during Arcing at varying pulse frequencies and heat input 7.28 kJ/cm.

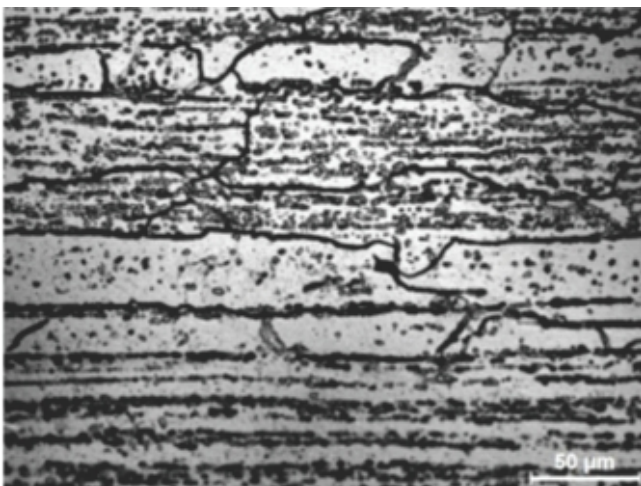


Fig. 12 : Typical microstructure of base metal

Fig. 12. It appears that the matrix primarily consists of banded grain structure of austenite aligned in the direction of rolling along with distribution of delta ferrite in it. The presence of delta ferrite appears to be in agreement to the Delong diagram that confirms the Chromium and Nickel equivalents as 14.3 and 4.7 respectively of base material composition (Table -II). At  $\phi = 0.4$  the effect of 'f' variation on fusion zone microstructure are shown for 2Hz at Fig. 13 (a) and for 6 Hz at Fig.13 (b). The microstructures show the presence of acicular and particulate delta ferrite network at grain boundary of the solidified fused matrix. It appears that the matrix morphology,

primarily with respect to the size of grains (growth of primary solid) and delta ferrite, is relatively finer at higher 'f' of 6 Hz. It also appears that at higher 'f' there is reduction in amount of ferrite transformation in the matrix.

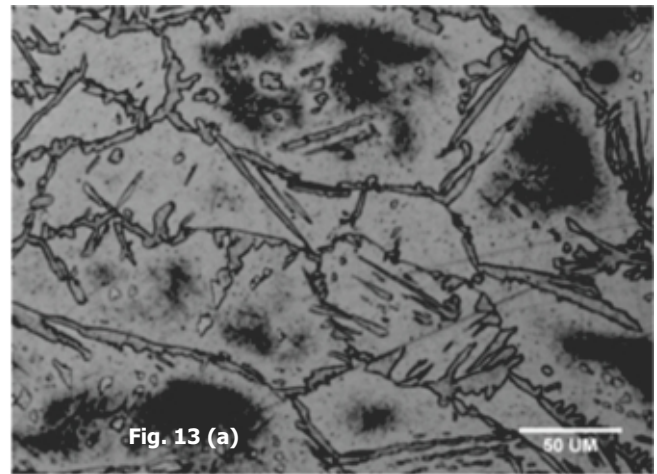


Fig. 13 (a)

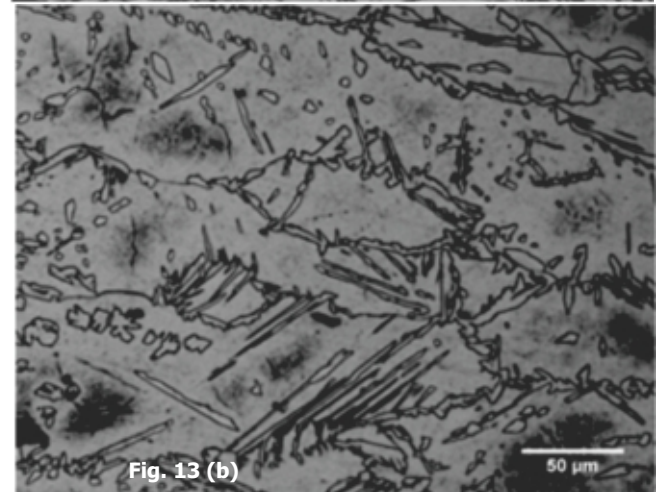


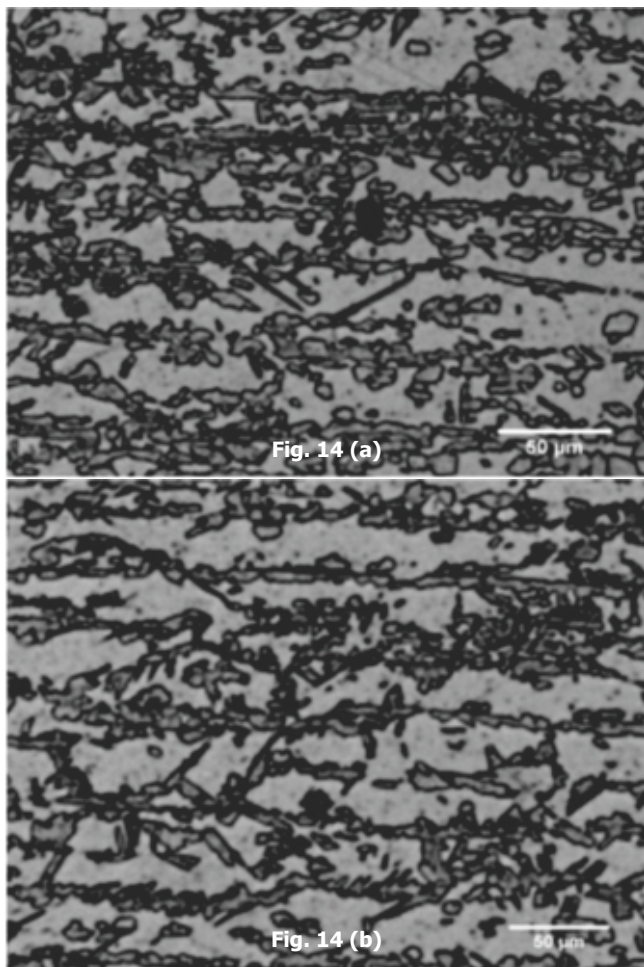
Fig. 13 (b)

Fig. 13 : At a given  $\phi = 0.4$  microstructure of fusion zone at pulse frequency (a) 2 Hz and (b) 6 Hz.

Such change of solidification behavior of fusion zone is well understood in the light of the increase of cooling rate and consequently faster primary solid growth when 'f' increased from 2 to 6 Hz at  $\phi = 0.4$  as discussed above in reference to Fig. 9 and 10 respectively.

At  $\phi = 0.4$  the effect of 'f' increase from 2 to 6 Hz on the microstructure of HAZ adjacent to the fusion zone has been shown in Fig. 14 (a) and (b) respectively. The microstructures show significant amount of particulate delta ferrite transformation in the matrix. It is noted that at constant ' $\phi$ ', the increase of 'f' to 6 Hz resulted in relatively less grain boundary ferrite transformation in the matrix than that

observed at  $f = 2$  Hz. Reason for such occurrence may be due to higher cooling rate of this region at 6 Hz along with that of the fusion zone (**Fig. 9**) as discussed above which has deprived the matrix from having more ferrite transformation.



**Fig. 14 :** At a given  $\phi=0.4$  microstructure of HAZ at pulse frequency (a) 2 Hz and (b) 6 Hz.

#### 4.5 Hardness at different modified zones

It has been observed that commensurate to the variation of microstructure, of fusion zone and HAZ adjacent to fusion zone of base material, their hardness values were also varied with change in 'f' and ' $\phi$ '. Hardness has always been found to increase with respect to that of the base material hardness of  $160 \pm 4$  HV. The nature of variation of average hardness at 1.85 mm depth of the fusion zone and the HAZ adjacent to the fusion zone with varying ' $\phi$ ' at different 'f' values are shown in **Fig. 15 (a) - (c)**. It appears that by keeping 'f' unchanged the increase of ' $\phi$ ' from 0.25 to 0.4 significantly improves hardness

at both the fusion zone and HAZ. Also keeping ' $\phi$ ' unchanged, increase relatively reduces the hardness of fusion zone and HAZ. With 'f' constant, the hardness increase of fusion zone with increase of ' $\phi$ ' was in agreement to its change of cooling rate (**Fig. 9**) and microstructure as discussed above. The maximum average hardness (210 HV) of fusion zone has been found at  $\phi = 0.4$  and pulse frequency of 2 Hz which is about 31% higher than that of the base material. Similarly the hardness of HAZ has been found to be raised up to about 231 HV which is also about 44% higher than that of the base material.

#### 5.0 CONCLUSION

Gas Tungsten pulse Arcing can be used as effective method for surface modification of martensitic stainless steel. The controlled fusion by Gas Tungsten Pulsed Arcing and its consequent thermal behavior has significant effect on the microstructure of fusion zone and HAZ. These micro structural changes improve surface hardness up to a significant depth of the relatively low hardness annealed SS410 stainless steel. The geometry and cooling rate of fusion zone and the HAZ can be varied by changing pulse frequency and ' $\phi$ ' (a dimensionless hypothetical factor containing different pulse parameters) at a given heat input. The use of a relatively low pulse frequency such as 2 Hz at  $\phi = 0.4$  increases the average hardness of fusion zone and HAZ by 31% and 44% respectively over that of the base material up to a depth of about 1.85 mm. The change in cooling characteristics of the matrix during solidification of the fusion zone is the reason for such hardness increase. The experiment was conducted in a particular material with some selected range of process parameters. There are scopes for further studies to ascertain the effect variation of process parameters on different material surfaces.

#### REFERENCES

- (1) Groning, P, Nowak, S. and Schlapbach, L. (1991). Temp. dependent surface modifications of AISI316L and AISI440C stainless steel substrates. *Appl Surf Sci*, 52(4), pp.333-337.
- (2) D'Oliveira, A.S.C.M., Paredes, R.S.C. and Santos, R.L.C. (2006) Pulsed current plasma transferred arc hardfacing. *J. of Mater Processing Technol*, 171(2), pp.167-174.
- (3) Hashimoto, M., Miyamoto, Y., Kubo, Y., Tokumaru, S., Ono, N., Takahasi, T. and Ito, I. (1995), *Surface*

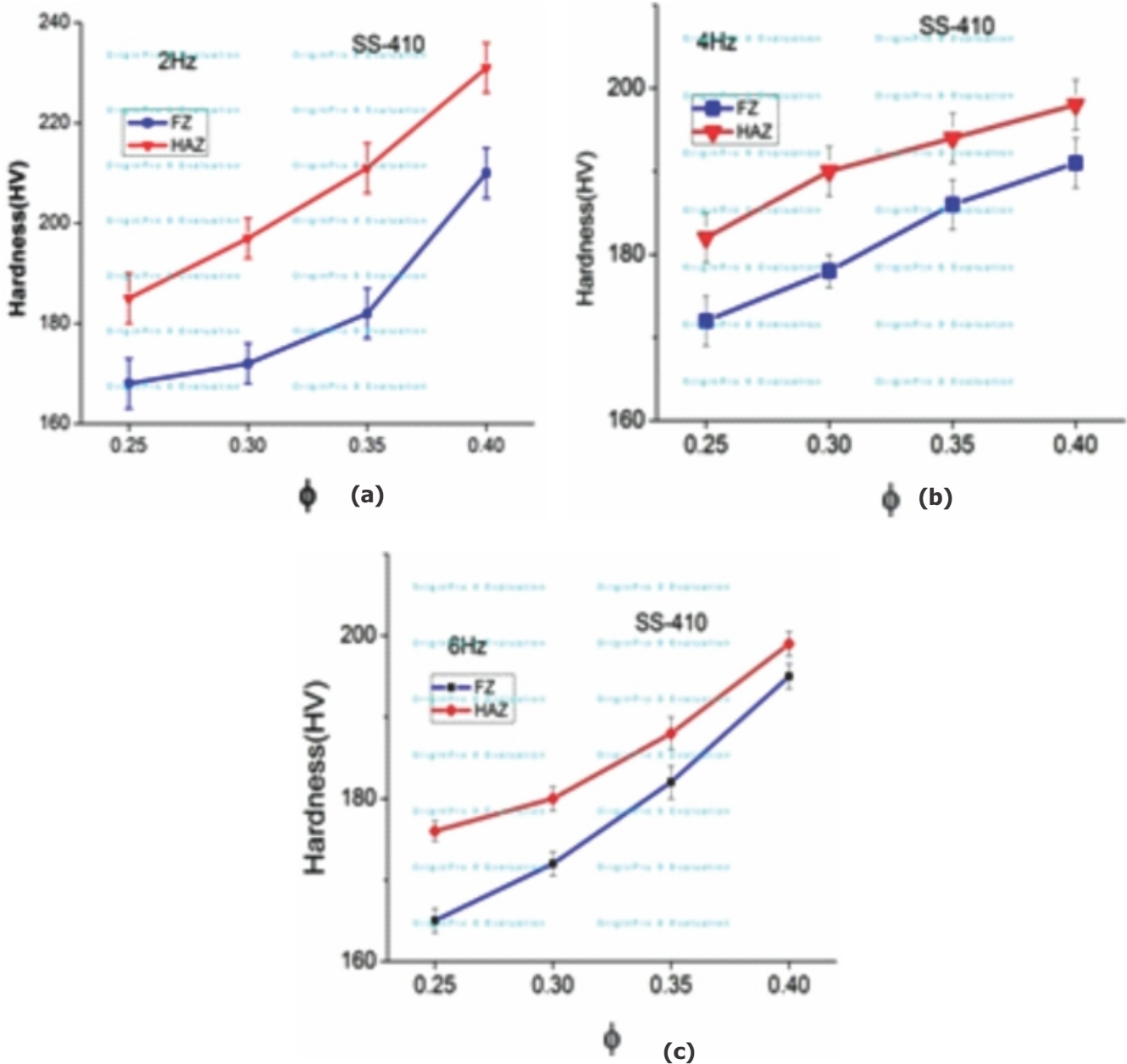


**Fig.15 : Effect of  $\phi$  on hardness of fusion zone and HAZ at pulse frequencies (a) 2Hz (b) 4Hz and (c) 6 Hz.**

modification of stainless steel in plasma environments, Mater Sc. & Eng, 198(1-2), pp.75-83.

- (4) Tsai, W., Shieh, C. and Lee, J. (1994) Surface modification of ferritic stainless steel by laser alloying, Thin Solid Films, 247(1), pp.79-84.
- (5) Kwok, C.T., Cheng, F.T. and Man, H.C. (2000) Laser surface modification of UNS S31603 stainless steel. Part I

: microstructures & corrosion characteristics, Mater Sc.& Eng, 290(1-2), pp.55-73.

- (6) Zou, J.X., Zhang, K.M., Hao, S.Z., Dong, C. and Grosdidier, T.,(2010). Mechanism of hardening, wear and corrosion improvement of 316L Stainless steel by low energy high current pulsed electron beam surface treatment, Thin Solid Films, 519(4), pp.1405-1415.

- (7) Steyer, P., Valette, S., Forest, B., Millet, J. P., Donnet, C. and Audouard, E. (2006) Surface modification of martensitic stainless steels by laser marking and its consequences regarding corrosion resistance, *Surf Eng*, 3, pp.167-172.
- (8) Pan, Q.Y., Huang, W.D., Song, R.G., Zhou, Y.H. and Zhang, G.L. (1998) The improvement of localized corrosion resistance in sensitized stainless steels by laser surface remelting, *Surf & Coatings Technol*, 102(3), pp.245-255.
- 9) Orłowicz, A.U. and Trytek, A. (2005), Use of the GTAW method for surface hardening of cast iron, *Weld International Res Suppl*, 19 (5), pp.341-348.
- (10) Ghosh, P.K. and Kumar, R. (2014) Surface modification of Micro-Alloyed high-strength low-alloy steel by controlled TIG arcing process, *The Minerals, Metals & Materials Society and ASM International*, doi:10.1007/s11661-014-2670-x.
- (11) Goyal, V.K. (2007), Effect of thermal and solidification behavior on characteristics of pulsed current GMA weld, Ph.D thesis, IIT, Roorkee, India
- (12) Ghosh, P.K., Goyal, V.K., Dhiman, H.K. and Kumar, M. (2006), Thermal and metal transfer behavior in pulsed current gas metal arc weld deposition of Al-Mg alloy, *Sci & technology of welding and joining*, 11(2), pp.232-242.
- (13) Poorhaydari, K., Patchett, B.M. and Ivey, D.G. (2005). Estimation of cooling rate in the welding of plates with intermediate thickness, *Weld Res*, October, pp.149-s-155-s.
- (14) Nguyen, N.T., Ohta, A., Matsuoka, K., Suzuki, N. and Maeda, Y. (1999), Analytical solutions for transient temperature of semi-infinite body subjected to 3-D moving heat sources, *Weld Res*, Aug, pp.265-s-274-s.